Direct and fast detection of neuronal activation in the human brain with diffusion MRI

Denis Le Bihan[†‡§], Shin-ichi Urayama[†], Toshihiko Aso[†], Takashi Hanakawa[†¶], and Hidenao Fukuyama[†]

[†]Human Brain Research Center, Kyoto University Graduate School of Medicine, Yoshida-Konoe-cho, Sakyo-ku, Kyoto 606-8501, Japan; [‡]Laboratory of Anatomical and Functional Neuroimaging, Service Hospitalier Frédéric Joliot, Commissariat à l'Energie Atomique, 4 Place du Général Leclerc, 91491 Orsay, France; and [¶]National Center of Neurology and Psychiatry, 4-1-1 Ogawahigashi, Kodaira, Tokyo 187-8502, Japan

Using MRI, we found that a slowly diffusing water pool was expanding (1.7 ± 0.3%) upon activation on the human visual cortex at the detriment of a faster diffusing pool. The time course of this water phase transition preceded the activation-triggered vascular response detected by usual functional MRI by several seconds. The observed changes in water diffusion likely reflect early biophysical events that take place in the activated cells, such as cell swelling and membrane expansion. Although the exact mechanisms remain to clarify, access to such an early and direct physiological marker of cortical activation with MRI will provide opportunities for functional neuroimaging of the human brain.

biophysics | brain activation | functional MRI | membrane | cell

Our current model of neuronal activation places great importance on transient electrical and biochemical events associated with the excitation processes. However, there is compelling evidence that activation is accompanied by other important physical phenomena. Microstructural changes in excited tissues have been observed, first from optical birefringence measurements (1, 2) and later more directly by using piezoelectric transducers (3). Those studies have revealed, for instance, that in the brain cell swelling is one of the physiological responses associated with neuronal activation (4, 5).

However, such biophysical events have been monitored at the microscopic level by using invasive techniques in neuronal cell cultures or slices, and do not necessarily reflect physiological conditions (6, 7). Observing changes in cortical cell configuration in animals or humans would, thus, have a tremendous impact, because they would be directly linked to neuronal events, such as membrane expansion, and bridge the gap with current approaches to obtain images of human brain activation. Those approaches, such as blood oxygen level-dependent (BOLD) MRI, are based on blood flow changes and only indirectly and remotely related to cortical activation (8, 9).

A small decrease of the water diffusion coefficient during activation of human visual cortex has been previously reported by using diffusion MRI (10). Diffusion MRI provides valuable information on the microscopic obstacles which hinder diffusing molecules, such as membranes or macromolecules, and in turn, on the tissue cellular structure (11). Based on other MRI reports of water diffusivity decrease during intense neuronal activation (12, 13) or during other physiological or pathological conditions inducing cell swelling (14–17), the observed diffusion findings have been putatively ascribed to a transient swelling of cortical cells and a shrinking of the extracellular space, increasing its tortuosity (18) for diffusing molecules. However, no confirmation has been found so far for this mechanism. The aim of this report is to demonstrate that a decrease in water mobility can readily been observed in the human brain with diffusion MRI upon activation, and to provide evidence that this effect results from an early neuronal activation event that precedes the blood flow response by a sizeable time amount. Results are interpreted in terms of a physical water phase transition in activated cells, and links with the physiological changes accompanying brain activation are discussed.

Results

Diffusion MRI Activation Maps. Diffusion MRI images from healthy volunteers were collected during visual stimulation with different degrees of diffusion sensitization. In all subjects, the activation maps directly calculated from the raw diffusion-sensitized MRI signals clearly showed activation of primary visual areas, as well as secondary visual areas, such as visual motion area MT/V5 which is often activated with flickering stimuli (19) (Fig. 1*A*). Higher-resolution images suggested that voxels detected as activated from diffusion MRI were well located along the cortical ribbon, whereas the BOLD functional MRI (fMRI) activated foci were much broader, encompassing large subcortical areas beyond the cortex (Fig. 1*B*). However, an in-depth comparison between diffusion and BOLD fMRI activation patterns was not the scope of this study which was solely focused on the characterization of the diffusion MRI signal source. Similarly, activated regions lying beyond early visual areas were not investigated.

As expected, the signal time course in a volume of interest (VOI) centered on the calcarine fissures exhibited an increase in the diffusion-sensitized signal (Fig. 2, see Fig. 3, which is published as supporting information on the PNAS web site). The results were noticeably better than in an earlier study (10), because of several critical improvements in the methods: (*i*) The study was performed at 3T by using an eight-channel phased-array coil, instead of a head coil at 1.5T, which provides a higher signal-to-noise ratio. (*ii*) As an important improvement to Darquie *et al.* (10), the diffusion MRI sequence was carefully chosen to be immune to background mesoscopic field gradients produced by local magnetic susceptibility inhomogeneities in the cortical tissue (20, 21). Such susceptibility effects can, in particular, be induced by paramagnetic blood deoxyhemoglobin and result in an artifactual underestimation of the diffusion coefficient measured with most diffusion MRI sequences (22, 23). With those sequences, as the concentration of deoxyhemoglobin decreases during cortical activation (24), a slight decrease of the diffusion-sensitized MRI signal is expected to mimic the BOLD signal time course (22) and to oppose the expected true diffusion-induced signal increase.

Functional Diffusion MRI. Although an increase in the diffusion-weighted MRI signal means an overall slowdown of the diffusion process, it cannot be converted to a drop of a water diffusion coefficient *per se*, as proposed in a simplified approach (10). Previous experimental studies (25) have well established that the water diffusion-sensitized MRI signal attenuation in brain tissue as a function of the degree of sensitization expressed is not linear, as would be expected for a free (Gaussian) diffusion behavior, but
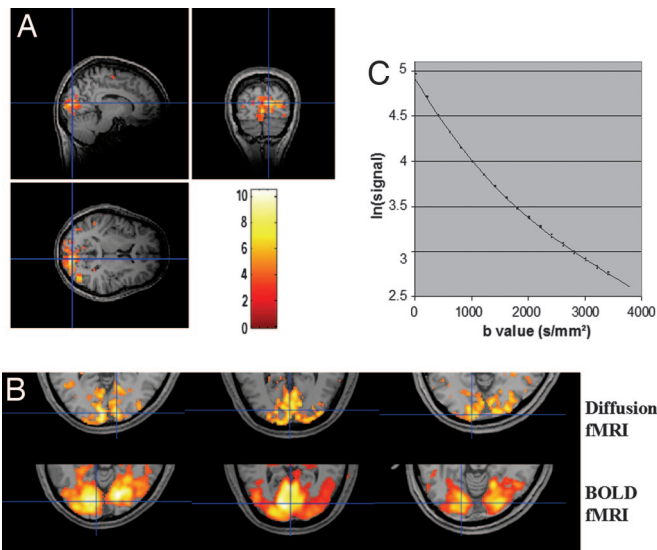
Fig. 1. Diffusion fMRI maps. (*A*) SPM activation map calculated from the *b* = 2,400 s/mm² diffusion-sensitized data set from one subject overlaid on a high-resolution anatomical MRI image. Areas in colors (*Z* score) correspond to voxels whose signal was significantly increased during visual activation. Beside the primary visual cortex region, activation of lateral MT/V5 can also be seen. (*B*) Zoom on the visual areas of three subjects from the SPM activation maps calculated with the high-resolution data sets (top row: *b* = 1,800 s/mm² diffusion-sensitized data set, bottom row, BOLD fMRI data set). Voxels detected as activated from diffusion MRI appear well located along the cortical ribbon, whereas BOLD fMRI foci detected with the same acquisition and processing parameters are much broader, encompassing large subcortical areas beyond the cortex. (*C*) Plot of the logarithm of the diffusion signal attenuation (with error bars) against *b* value (degree of diffusion sensitization) from the visually activated VOI of subject of *A*. This plot is expected to be linear in the case of unrestricted diffusion in a homogeneous compartment. The plot clearly shows a curvature, which was modeled by using a biexponential function, corresponding to a fast and a slow water diffusion phase.

curved, so that in the brain, diffusion cannot be accurately described in terms of a single diffusion coefficient.

Water biphasic model. To shed light on the observed changes in water diffusion we have used a biphasic diffusion model of the brain cortex that accounts for this curvature behavior. Earlier studies (25) have shown that the diffusion MRI signal curvature could be very well fitted with a biexponential function corresponding to a slow diffusion phase (SDP) and a fast diffusion phase (FDP) in slow exchange

$$S = S_0 f_{\text{slow}} \exp(-b D_{\text{slow}}) + S_0 f_{\text{fast}} \exp(-b D_{\text{fast}}), \quad [1]$$

where *b* is the degree of diffusion sensitisation (so called "*b* value"; ref. 11), *S* is the MRI signal at a particular *b* value, S_0 is the signal at *b* = 0, *f* and *D* are the MRI visible volume fractions and the diffusion coefficients associated to the slow and fast diffusion phases, with $f_{\text{slow}} + f_{\text{fast}} = 1$.

The volume fractions of the FDP and SDP (respectively ≈70% and 30%) do not match on a static basis the volume fractions of the extra- and intracellular compartments (26), so that the FDP and the SDP cannot be directly identified to those physical compartments. Models reflecting dynamic parameters, such as membrane restriction and permeability (27), and geometrical features (28) have been considered, but those distinct models lead to a diffusion signal decay which is nevertheless well approximated by a biexponential function (29–32). Indeed, the estimates for the diffusion coefficients and the respective volume fractions of the SDP and FDP have been strikingly consistent across literature (33–35). Hence, unsurprisingly, the diffusion data that we obtained at different *b* values in a

resting condition (Fig. 1*C*) in the visual cortex of our subjects and fitted with Eq. **1** gave very reproducible results, in very good agreement with those literature values (Table 1).

Functional diffusion model. More interestingly, on the other hand, there is experimental evidence that the respective volume variations of the SDP and FDP correlate very well with the volume variations of the intra- and extracellular spaces which result from cell swelling or shrinking in different physiological, pathological or experimental conditions (14–17, 25). Hence, until a more comprehensive water diffusion model becomes available this biexponential description of tissue water diffusion remains a robust and simple way to describe diffusion MRI data and, in its differential form, to address changes in tissue water distribution. Assuming small signal variations the relative signal change, dS/S, can be modeled as:

$$dS/S = F_{\text{slow}} df_{\text{slow}} + F_{\text{fast}} df_{\text{fast}}, \text{ where } F_{\text{i=fast,slow}} = \exp(-b D_{\text{i}})/$$

$$[f_{\text{slow}} \exp(-b D_{\text{slow}}) + f_{\text{fast}} \exp(-b D_{\text{fast}})]. \quad [2]$$

$df_{\text{slow, fast}}$ is the change in volume fraction of the slow and fast diffusion phases resulting from activation. Variations of S_0, D_{slow}, and D_{fast} were found to be of second order, if any, in agreement with literature (17).

The diffusion data obtained during activation at different *b* values were analyzed according to this SDP/FDP functional diffusion model. The first important result was that the diffusion MRI signal change increased, almost linearly, with the *b* value and significantly in all subjects (Fig. 2*A*; see Fig. 4, which is published as supporting information on the PNAS web site). Using the diffusion parameters determined in the activated VOI of each subject from the diffusion data set acquired in the resting state, we could estimate the amount of changes of the SDP and FDP volumes induced by activation by fitting the observed variations in dS/S for each *b* value with the model. Only changes in the SDP and FDP volume fractions could match the observed response increase with *b* values ($P < 0.02$ for each individual subject), whereas variations in the SDP and FDP diffusion coefficients could not yield the observed amount of signal increase. The results were remarkably consistent across all subjects (Table 1), with a SDP expansion by +0.56 ± 0.07% of the MRI-visible water content and a FDP decrease by −0.44 ± 0.12%. Noticeably, the difference in amounts between the SDP expansion and the FDP decrease was not statistically different. Because these parameters were estimated without any *a priori* constraint on a possible relationship between them these results strongly suggest that, although the VOI's total amount of water remained constant (no compression) upon activation, 0.5% of the VOI's (MRI-visible) water experienced a transition from the fast-diffusing phase to the slow-diffusion phase. Taking into account the SDP size, this amount translated to an activation-induced relative increase of 1.7 ± 0.3% of the slow diffusion phase (Table 1). Partial volume effects have likely arisen between the activated and nonactivated tissues in some voxels, given the spatial resolution of the images. Therefore, only a fraction of the cells present in the VOI experienced this water phase transition, so that local SDP expansion would likely be much higher in some cell clusters. In summary, according to this functional diffusion model, our results suggest that the transient water diffusion decrease observed upon activation primarily results from a water phase transition, and not from the decrease of a diffusion coefficient which could have resulted from an increase of tortuosity in the extracellular space (10).

Diffusion MRI Time Course. To further characterize the nature of this water phase-transition, the SDP expansion time course during activation was also investigated. Although the raw diffusion-sensitized signal time courses could have been directly used (without resorting to the above functional diffusion model), we transformed the signal time course at each *b* value into a SDP expansion

Le Bihan *et al.*

Fig. 2. Amplitude and time course analysis. (*A Left*) Plots of the relative signal increase $dS/S = f(b)$ for the VOI of one representative subject ($\pm$SD for each data point, statistical *t* test comparing pairs of *b* values; ns, not significant; *, $P < 0.05$; **, $P < 0.01$; ***, $P < 0.001$). The red curve corresponds to the theoretical signal increase expected from the biphasic diffusion model with parameters adjusted to the data. (*A Center*) Time courses of the SDP expansion amount (red) and of the normalized BOLD fMRI signal (blue) of one subject. The BOLD signal time course exhibits a shallow ''initial dip'' and a poststimulus undershoot. By contrast, the SDP time course presents a steeper onset without any initial dip. Although the BOLD and SDP time courses are very similar in shape, the SPD time course is always ahead of the BOLD time course. This diffusion advance is mostly noticeable at the beginning of the activation response. (*A Right*) Normalized rms difference, nRMS(Δt), between the diffusion-derived SDP swelling time course and the BOLD signal time course shifted by a time interval Δt (U-shape curve, nRMS; bottom curve, temporal derivative). nRMS is minimized for $\Delta t < 0$, as best seen from the zero-crossing of the nRMS(Δt) temporal derivative. (*B Left*) Time courses of the diffusion MRI ($b = 0$, 250 and 1,800 s/mm^2) and the BOLD fMRI signals with the box-car activation paradigm of one representative subject (left, raw signal change; right, normalized signal change). A large advance of the MRI signal with high diffusion sensitization ($b = 1,800$ s/mm^2) over the BOLD response can be seen, both at onset and offset. The diffusion MRI response appears well locked to the activation paradigm, whereas the BOLD fMRI response is shifted by several seconds. On the other hand, the increase signal observed without diffusion sensitization ($b = 0$ s/mm^2) shows a time course perfectly synchronized with the BOLD response. The signal change observed at low diffusion-sensitization ($b = 250$ s/mm^2) is significantly lower than that seen at high *b* value. At low diffusion-sensitization, the signal time course mixes the diffusion time course observed at higher *b* value (early onset) with that of the vascular, BOLD component (late offset) which is totally removed at $b = 1,800$ s/mm^2. (*B Right*) Normalized rms difference, nRMS(Δt), between the BOLD signal time course shifted by a time interval Δt and the $b = 1,800$ s/mm^2 diffusion MRI signal time course (left) or the $b = 0$ s/mm^2 diffusion MRI signal time course (right). Although the $b = 0$ s/mm^2 and BOLD time course exactly coincide ($\Delta t = 0$), the nRMS between $b = 1,800$ s/mm^2 diffusion MRI and BOLD time courses is clearly minimized for $\Delta t < 0$.

time course. According to the functional diffusion model, the expansion amount no longer depends on *b* values, and the VOI signal from all data sets can be merged into a single SDP expansion time course to provide a better signal-to-noise ratio. In line with the above results (phase-transition), the decrease in the fast volume fraction was assumed to balance the increase in the slow volume fraction, i.e., $df_{fast} = -df_{slow}$, so that the relative change of the slow diffusion phase volume, df_{slow}/f_{slow}, could be directly calculated from the signal change, dS/S:

$$df_{slow}/f_{slow} = K\,dS/S, \text{ where } K = [f_{slow}\exp(-bD_{slow})$$
$$+ (1 - f_{slow})\exp(-bD_{fast})]/$$
$$\{f_{slow}[\exp(-bD_{slow}) - \exp(-bD_{fast})]\}. \quad [3]$$

A comparison was made with the usual BOLD fMRI signal time course extracted from the VOI of each subject. In agreement with

literature (36), the BOLD signal time course exhibited a shallow "initial dip" and a poststimulus undershoot (Fig. 2*A*; see Fig. 5, which is published as supporting information on the PNAS web site). By contrast, the diffusion-derived SDP expansion time course showed a sharp increase at stimulus onset, but neither any initial dip nor any clear poststimulus undershoot. Overall, the BOLD and SDP expansion time courses were very similar in shape. However, the most striking feature was that the SDP time course was always ahead of the BOLD time course by several seconds, most noticeably at the beginning of the activation period, but often also at its end. To quantify the advance of the SDP response, the BOLD time course was shifted in time, and a normalized rms difference (nRMS) was calculated between the SDP and the time-shifted BOLD time course (Fig. 2*A*; see Fig. 6, which is published as supporting information on the PNAS web site). The nRMS minimum value provided an estimate of the time delay, which made both time courses mostly similar. This delay was very consistent across all

NEUROSCIENCE

Table 1. Data from all subjects

Subject	VOI size, voxels	SDP fraction, %	df_{slow}, %	SDP swelling amount, %*	BOLD signal increase, %	df_{fast}, %	[SDP swelling-BOLD] time shift, s
Ta . . .	72	35.2	0.50 ± 0.06	1.4	2.3	-0.35 ± 0.23	-1.9 ± 0.5
Na . . .	127	34.1	0.65 ± 0.05	1.9	2.8	-0.40 ± 0.22	-2.2 ± 0.5
Hi . . .	127	34.0	0.49 ± 0.06	1.4	2.4	-0.52 ± 0.23	-2.2 ± 0.5
Ba . . .	90	29.9	0.62 ± 0.10	2.1	2.3	-0.64 ± 0.33	-1.9 ± 0.5
Ya . . .	146	32.2	0.50 ± 0.06	1.5	2.8	-0.34 ± 0.30	-3.2 ± 0.5
Ch . . .	175	34.0	0.60 ± 0.10	1.8	1.7	-0.37 ± 0.36	-3.2 ± 0.5
Mean	123 ± 38	33.1 ± 2.1	0.56 ± 0.07	1.7 ± 0.3	2.4 ± 0.4	-0.44 ± 0.12	-2.4 ± 0.7

*Slow diffusion pool swelling amount was calculated as df_{slow}/f_{slow}

our subjects, with the diffusion-derived SDP response preceding the BOLD response by an average of 2.4 ± 0.7 s (Table 1).

This major result clearly demonstrates that the observed diffusion changes and the BOLD effect refer to rather different physiological events underlying cortical activation. The BOLD effect has been shown to originate from local changes in the blood deoxyhemoglobin concentration, which mainly result from the increase in blood flow and blood volume induced by neuronal activation (24, 36). Therefore, it is a vascular event and, although BOLD fMRI has been extremely successful for the functional neuroimaging community, presents well known limitations. Although the existence of a coupling between neuronal activation, metabolism, and blood flow has been verified in most instances including BOLD fMRI (9), the degree and the mechanism of coupling remain largely not understood (37). This is an important concern for the application of fMRI in the clinical field, because this coupling might fail in some disease cases (38). Also, it has been pointed out that the spatial functional resolution of BOLD fMRI might be limited, because vessels responsible for the increase of blood flow and blood volume feed or drain somewhat large territories, whereas the physiological delay necessary for the mechanisms triggering the vascular response to work intrinsically limits the temporal resolution of BOLD fMRI.

Origin of the Observed MRI Signal Changes. *Water diffusion origin.* The significant variations of the observed signal responses upon activation with the amount of diffusion sensitization (b values) sign their diffusion origin. Residual BOLD effects could also mimic diffusion effects through variations in the magnetic susceptibility-induced local field gradients, as noted above, but such effects should be completely negligible given the particular diffusion sequence used in this study, which is confirmed by the clear time difference between the diffusion and the BOLD time courses. However, it remains that small BOLD induced signal variations due to changes in R2/R2* relaxation in intravascular blood have been reported when using spin-echo sequences with very low b values (39). To evaluate such residual contribution, and to further provide evidence of the nonvascular origin of the diffusion MRI changes, control acquisitions were obtained with a higher spatial resolution and a shorter stimulation duration to enhance the time differences between the diffusion and BOLD effects. The results confirm the large advance of the MRI signal with high diffusion sensitization ($b = 1,800$ s/mm^2) (up to 4 s) over the BOLD response (Fig. 2B, Table 2, and Fig. 7, which is published as supporting information on

the PNAS web site), even larger than with a longer stimulus (Fig. 2A). On the other hand, the signal increase, which is seen with the spin-echo sequence without diffusion sensitization ($b = 0$ s/mm^2), has a time course that perfectly matches the BOLD response, so that one may reasonably think it shares its vascular origin. This finding is further confirmed by the significant decrease in signal response observed when adding a small amount of diffusion-sensitization ($b = 250$ s/mm^2). The magnetic field gradient pulses used for diffusion sensitization also induce velocity-dependent phase shifts in the presence of flow and suppress signal from flowing blood due to the intravoxel incoherent motion effect (40). Adding a small degree of diffusion sensitization, therefore, "crushes" the vascular component of the BOLD signal (39). Very interestingly, at $b = 250$ s/mm^2, the signal temporal profile mixed the diffusion time course observed at higher b values (early onset) with a residual vascular (BOLD) component (late offset), which is totally removed at higher b values. The signal change at $b = 1,800$ s/mm^2 was significantly larger than that observed at $b = 250$ s/mm^2 (Table 2), in line with the other results of this report. In addition, there was no correlation (Table 1, $r = -0.11$) between the amplitude of the SDP expansion and that of the BOLD signal, as measured before normalization, further supporting the fact that the diffusion-derived signal and the BOLD response have different origins. In summary, those results confirm that (*i*) the observed signal changes have a true diffusion origin and (*ii*) the mechanism of the diffusion response is not vascular.

Link with cell physiology. In the brain, cell swelling is an important physiological response associated with neuronal activation (4, 7, 41–43). Such swelling not only involves neuronal soma, but also axons and focal areas along dendrites (42, 44), and probably also glial cells (45). The amount of swelling cannot be ascribed to a simple translocation of water from the extra to the intracellular space to compensate for fluctuations in intracellular osmolarity due to transient fluxes of ions (46), and further studies have underlined the importance of the cytoskeleton, a dense polymer-gel matrix running contiguously to the cell membrane (43, 47). Therefore, cortical cell swelling and its active regulation appear of fundamental importance to neuronal function. Interestingly, swelling and membrane expansion have been shown to start simultaneously with the electric response and the peak of the mechanical response to coincide accurately with the action potential peak. The response is asymmetric, as the swelling presents a sharp increase, whereas the return to baseline is smooth and monotonic (43, 48). Because the

Table 2. High-resolution and control data

Subject	$b = 0$ signal change, %	$b = 250$ signal change, %	$b = 1,800$ signal change, %	$b = 1,800/$ $b = 250$ (t test)	BOLD signal change, %	[$b = 1,800$-BOLD] time shift, s	[$b = 0$-BOLD] time shift, s
1	0.96 ± 0.06	0.69 ± 0.09	2.02 ± 0.18	$P < 5.10^{-5}$	2.07 ± 0.07	-2.7 ± 0.8	-0.0 ± 0.8
2	1.15 ± 0.07	0.64 ± 0.11	1.73 ± 0.27	$P < 2.10^{-4}$	2.02 ± 0.18	-3.0 ± 0.8	-0.0 ± 0.8
3	0.54 ± 0.13	0.33 ± 0.08	1.91 ± 0.28	$P < 5.10^{-5}$	1.53 ± 0.12	-4.0 ± 0.8	-0.1 ± 0.8

Le Bihan *et al.*

www.manaraa.com

diffusion-derived SDP response preceded the BOLD response by a sizeable time interval, there is strong indication that the SDP expansion is correlated with such an early neuronal activation event, which directly or indirectly triggers the vascular response, later revealed up by the BOLD effect.

The important role of water movements and water structuring within the membrane-bound polymer-gel matrix, which contains a high density of macromolecules has already been acknowledged (2, 43, 49). The deviation of the water diffusion decay in brain tissue from a single exponential function is known to result from the presence of diffusion barriers in the tissue, mainly cell membranes (32). One could speculate, then, that the SDP originates from layers of water molecules that are the most hindered in their motion and, thus, mainly in close contact with cell membranes that exhibit long range protein-trapping effects (50). The link of the SDP with the membrane-bound water pool is also supported by the observation that the SDP volume fraction is anisotropic in oriented tissues, such as brain white matter (35): the SDP fraction appears larger when diffusion measurements are made in a direction which maximizes membrane surface intersections, e.g., when diffusion is measured perpendicularly to white matter fibers. Therefore, the SDP should be considered more as a functional phase of "trapped" water rather than a definite physical compartment. Any fluctuation in cell size would induce a large variation of the membrane-bound water phase layer, making diffusion-sensitized MRI very sensitive to cell size variations, as confirmed in the literature (14–17, 25, 51). Clearly, a more comprehensive model of water–membrane interactions and their relationship with cortical cell physiology is needed before the reported results could be fully appreciated.

Conclusion

This study reveals that an early physiological marker of neuronal activation can be monitored to produce maps of cortical activation in the human brain with diffusion-sensitized MRI. This marker, a water-phase transition, reflects neuronal activation faster and more directly than the usual hemodynamic response detected with BOLD fMRI, offering a unique approach for brain functional studies. The diffusion-sensitized MRI signal can be converted into the expanse of a slow diffusion cortical water phase and quantified. Interestingly, the observed changes in water diffusion likely reflect biophysical events that actually take place in the activated cells and might physiologically contribute to the activation mechanisms. Therefore, one might expect that this approach, which can be applied in the brain of intact animals and humans, would provide new opportunities to understand the elementary processes underlying cortical activation or the existence of "nonsynaptic" mechanisms (52, 53). However, many issues remain to be investigated: although the observed water-phase transition could be linked to the expansion of a membrane bound-water phase, the physical nature of the fast and slow diffusion water phases and the relationship between their volume variations and cell swelling, as well as the biophysical mechanisms underlying the swelling in terms of ion/water fluxes and cytoskeleton involvement must be clarified. The time course of the swelling upon activation should thus be investigated with a higher resolution and directly compared with data obtained from electrical or optical recordings. Further improvements, such as event-related paradigms with a stimulus onset jitter, would provide opportunities to fully exploit the potential temporal resolution of diffusion fMRI. Fine localization of the SDP swelling within and along the cortical ribbon should also been looked at and compared with the BOLD hemodynamic response in terms of spatial accuracy. Such studies would benefit from enhancements in the sensitivity of diffusion-sensitized MRI to activation, for instance by applying larger diffusion sensitization through higher b values, combined with the increase in signal-to-noise ratio expected from MRI scanners operating at very high field.

Le Bihan *et al.*

Materials and Methods

Data Collection. The IRB approved study was performed on six volunteers (three males, three females, age 24–27) using a 3T whole-body MRI scanner equipped with an eight-channel phased-array head coil and a 40-mTm^{-1} actively shielded gradient coil (Siemens, Erlangen, Germany). Eight oblique slices centered on calcarine fissure were selected from a rapid localization scan. To minimize residual susceptibility effects the diffusion fMRI sequence (data set A) consisted in a twice refocused spin-echo echo-planar imaging (EPI) sequence sensitized to diffusion by an interleaved pair of bipolar magnetic field gradient pulses (20, 21). Acquisition parameters were as follows: slice thickness = 3.8 mm with 50% gap, pixel size = 3.75^2 mm^2, generalized autocalibrating partially parallel acquisitions (GRAPPA) with 2-fold acceleration, 87 ms echo time, 1 s repetition time, 1,302 Hz bandwidth. Four b values were chosen to spawn the widest range possible of b values technically compatible with our MRI scanner while keeping the acquisition length of the whole experiment within reasonable limits (b = 600, 1,200, 1,800, and 2,400 s/mm^2, with gradient pulses simultaneously applied along x, y, and z axes). The acquisitions were repeated three times in random order for each of the four b values to increase signal-to-noise ratio for the diffusion model fitting resulting in a total number of 12 sets. Although diffusion anisotropy was not expected in brain cortex (11), the polarity of the gradient pulses along x axis was inverted in half the subjects. BOLD fMRI images (data set B) were acquired by using a gradient-echo sequence with the same parameters, except for a 30 ms echo time. For both fMRI experiments, visual stimulation was obtained from a flickering dartboard (frequency, 8 Hz) projected on a screen within the MRI scanner room through a video projector. The activation paradigm consisted of three epochs of 20 (or 16) s separated by a 20-s (or 24-s) interval. At the end of the fMRI experiment, a high-resolution anatomical acquisition scan (data set C) was run for registration purposes using a three-dimensional magnetization-prepared rapid gradient-echo T1-weighted sequence (0.94 × 0.94 × 0.95 mm^3 voxels, 2 s repetition time, 4.38 ms echo time, 990 ms inversion time, 8° flip angle, 130 Hz bandwidth). Finally, a set of 18 diffusion-sensitized images (data set D) was also acquired in a resting condition with b values ranging from 0 to 3,400 s/mm^2 using a 200 s/mm^2 increment to perform a diffusion pool analysis. The acquisition was repeated 16 times to increase signal-to-noise ratio. Total scan time was 50 min.

In addition the acquisition protocol was repeated with slightly modified parameters to accommodate a higher spatial resolution (2 × 2 × 3 mm^3, with an echo time of 93 ms and a repetition time of 1.5 s) for the diffusion and BOLD data sets (respectively A$_{high}$ and B$_{high}$). In three of the subjects, the diffusion fMRI sequence (data set A$_{high}$) was run with only one b value (b = 1,800 s/mm^2), but repeated 10 times to increase signal-to-noise ratio and provide a higher spatial resolution in the activation maps (Fig. 1B). In three other subjects, the stimulation epochs were shortened to 10.5 s (repeated four times) for data sets A$_{high}$ and B$_{high}$ to provide a better temporal differentiation of the diffusion and BOLD fMRI signals. In this case, the data set A$_{high}$ consisted of three b values (b = 0, 250, and 1,800 s/mm^2), each repeated three times. The low b values were included as a control to evaluate residual BOLD effects (Fig. 2).

Functional Diffusion MRI Processing. Activation maps were calculated individually for each subject from the b = 2,400 s/mm^2 diffusion-sensitized fMRI images of data set A using SPM5 software (www.fil.ion.ucl.ac.uk/spm). Images were first corrected for motion and registered to the high-resolution anatomical images followed by spatial smoothing with a Gaussian filter (6 mm full width at half maximum). The choice for the b = 2,400 s/mm^2 diffusion data set was motivated by its highest sensitivity to activation (Fig. 2A). For each subject, a 30-mm half-sphere was selected to cover both

calcarine fissures. Within this sphere, a VOI was defined from the voxels classified as activated from the $b = 2,400$ s/mm^2 activation map ($P < 0.001$, uncorrected for multiple comparisons). This diffusion-defined VOI was then used subsequently to extract data from all diffusion and BOLD sets (data sets A, B, and D). The size of the VOI for each subject is given in Table 1. The same SPM analysis was performed on the $b = 1,800$ s/mm^2 diffusion-sensitized fMRI images of data set A$_{high}$ and the BOLD fMRI images of data set B$_{high}$ (Fig. 2), but with a boxcar basis function to avoid any bias.

Diffusion Pool Analysis. The VOI averaged signal from the images of data set D was extracted for each of the 18 b values and for each individual subject. The resulting signal, S, was averaged over the 16 diffusion acquisitions and plotted against the b value for each subject (Fig. 1C) (35). The first three points were discarded to avoid possible partial volume effects from cerebrospinal fluid. A nonlinear Marquardt algorithm was used to estimate from the diffusion-sensitized signal at each b value the diffusion parameters, f and D, of the slow and fast diffusion phases in resting condition for each subject VOI according to the biexponential model (Eq. 1).

Diffusion Functional Model Processing. The VOI averaged signal time course from data set A was extracted for each individual b value (600, 1,200, 1,800, and 2,400 s/mm^2). The resulting signal was averaged over the three acquisitions acquired at each b value, linearly corrected for any baseline drift for each b value (Fig. 1C). The signal from the resting and activated conditions were then pooled separately to estimate the signal change (dS/S) induced by activation for each b value. A least-squares bilinear fitting algorithm was used to estimate the respective changes, df_{slow} and df_{fast}, from the signal changes, dS/S, observed for each b value (Eq. 2) and the diffusion parameters previously determined for the VOI of each subject. Both parameters were considered *a priori* as free (without the $f_{slow} + f_{fast} = 1$ constraint). The observed and the predicted signal changes, dS/S, were plotted against b values for each subject VOI (Fig. 2).

Time Course Analysis. The VOI averaged, b value averaged, baseline drift corrected signal time course for each b value of data set A was then folded into a single [activation − rest] epoch by averaging the three subsequent epochs of the paradigm. The [dS/S](t) time course for each b value was transformed into a [df_{slow}/df_{slow}](t) time course (Eq. 3), with [dS/S](t) defined as $S(t)/S$(baseline) − 1. S(baseline) was obtained by averaging signal during the resting condition. Because df_{slow}/df_{slow} is now a physiological parameter that does not depend on the b value, the [df_{slow}/df_{slow}](t) time courses were averaged over the four b values.

For comparison, the averaged BOLD fMRI signal time course was extracted from data set B using the diffusion-defined VOI of each subject and linearly corrected for any baseline drift. The raw BOLD fMRI signal time course was expressed as a relative change to baseline, [dS_{BOLD}/S_{BOLD}](t), defined as $S_{BOLD}(t)/S_{BOLD}$(baseline) − 1. S_{BOLD}(baseline) was obtained by averaging signal during the resting condition. The BOLD fMRI time course was then folded into a single [activation − rest] epoch by averaging the three subsequent epochs of the paradigm. Finally, as the BOLD fMRI signal intensity is arbitrary the [dS_{BOLD}/S_{BOLD}](t) time course was normalized, so that, for timing comparison only, the amplitude of its envelope matched that of the [df_{slow}/df_{slow}](t) time course. The normalized [dS_{BOLD}/S_{BOLD}](t) and the [df_{slow}/df_{slow}](t) time courses were finally plotted together for the VOI of each subject (Fig. 2A).

To obtain a quantitative estimation of the time shift between the [df_{slow}/df_{slow}](t) and the [dS_{BOLD}/S_{BOLD}](t) time courses, the BOLD fMRI time course was shifted by a time interval Δt from −6 to +4 s. The resulting [dS_{BOLD}/S_{BOLD}]($t + \Delta t$) time course was compared with the [df_{slow}/df_{slow}](t) time course by calculating the normalized rms difference, nRMS(Δt), between the activated epochs of the two time courses, which was plotted against Δt (Fig. 2A). The time shift minimizing the differences between the [df_{slow}/df_{slow}](t) and [dS_{BOLD}/S_{BOLD}](t) time courses was estimated from the lowest nRMS value, as derived from the zero-crossing of its time derivative. The same processing was performed on the A$_{high}$ and B$_{high}$ data sets to compare the time courses of the BOLD and $b = 1,800$ s/mm^2 diffusion data sets on one hand, and of the BOLD and $b = 0$ s/mm^2 diffusion data sets on the other hand (Fig. 2B).

1. Cohen, L. B., Keynes, R. D. & Hille, B. (1968) *Nature* **218,** 438–441.
2. Tasaki, I. & Byrne, P. M. (1993) *Jpn. J. Physiol.* **43,** Suppl. 1, S67–S75.
3. Tasaki, I. & Iwasa, K. (1982) *Jpn. J Physiol.* **32,** 69–81.
4. Andrew, R. D. & Macvicar, B. A. (1994) *Neuroscience* **62,** 371–383.
5. Schwartzkroin, P. A., Baraban, S. C. & Hochman, D. W. (1998) *Epilepsy Res.* **32,** 275–285.
6. Sykova, E., Vargova, L., Kubinova, D., Jendelova, P. & Chvatal, A. (2003) *NeuroImage* **18,** 214–230.
7. Holthoff, K. & Witte, O. W. (1996) *J. Neurosci.* **16,** 2740–2749.
8. Ogawa, S., Tank, D. W., Menon, R. S., Ellerman, J. M., Kim, S. G., Merkle, H. & Ugurbil, K. (1992) *Proc. Natl. Acad. Sci. USA* **89,** 5951–5955.
9. Logothetis, N. K., Pauls, J., Augath, M., Trinath, T. & Oeltermann, A. (2001) *Nature* **412,** 150–157.
10. Darquie, A., Poline, J. B., Poupon, C., Saint-Jalmes, H. & Le Bihan, D. (2001) *Proc. Natl. Acad. Sci. USA* **98,** 9391–9395.
11. Le Bihan, D. (2003) *Nat. Rev. Neurosci.* **4,** 469–480.
12. Zhong, J., Petroff, O. A. C., Pleban, L. A., Gore, J. C. & Prichard, J. W. (1997) *Magn. Reson. Med.* **37,** 1–6.
13. Latour, L., Hasegawa, Y., Formato, J. E., Fisher, M. & Sotak, C. H. (1994) *Magn. Reson. Med.* **32,** 189–198.
14. O'Shea, J. M., Williams, S. R., van Bruggen, N. & Gardner-Medwin, A. R. (2000) *Magn. Reson. Med.* **44,** 427–432.
15. Hasegawa, Y., Formato, J. E., Latour, L. L., Gutierrez, J. A., Liu, K. F., Garcia, J. H., Sotak, C. H. & Fisher, M. (1996) *Stroke* **27,** 1648–1655.
16. Van Der Toorn, A., Sykova, E., Dijkhuizen, R. M., Vorisek, I., Vargova, L., Skobisova, E., Van Lookeren Campagne, M., Reese, T. & Nicolay, K. (1996) *Magn. Reson. Med.* **36,** 52–60.
17. Buckley, D. L., Bui, J. D., Phillips, M. I., Zelles, T., Inglis, B. A., Plant, H. D. & Blackband, S. J. (1999) *Magn. Reson. Med.* **41,** 137–142.
18. Chen, K. C. & Nicholson, C. (2000) *Proc. Natl. Acad. Sci. USA* **97,** 8306–8311.
19. Kubova, J., Kuba, M., Spekreijse, H. & Blakemore, C. (1995) *Vision Res.* **35,** 197–205.
20. Reese, T. G., Heid, O., Weisskoff, R. M. & Wedeen, V. J. (2003) *Magn. Reson. Med.* **49,** 177–182.
21. Karlicek, R. F. & Lowe, I. J. (1980) *J. Magn. Reson.* **37,** 75–91.
22. Does, M. D., Zhong, J. & Gore, J. C. (1999) *Magn. Reson. Med.* **41,** 236–240.
23. Kiselev, V. G. (2004) *J. Magn. Reson.* **170,** 228–235.
24. Ogawa, S., Menon, R. S., Tank, D. W., Kim, S. G., Merkle, H., Ellermann, J. M. & Ugurbil, K. (1993) *Biophys. J.* **64,** 803–808.
25. Niendorf, T., Dijkhuizen, R. M., Norris, D. G., Van Lookeren Campagne, M. & Nicolay, K. (1996) *Magn. Reson. Med.* **36,** 847–857.
26. Sehy, J. V., Ackerman, J. J. H. & Neil, J. J. (2002) *Magn. Reson. Med.* **48,** 765–770.
27. Novikov, E. G., Van Dusschoten, D. & VanAs, H. (1998) *J. Magn. Reson.* **135,** 522–528.
28. vanderWeerd, L., Melnikov, S. M., Vergeldt, F. J., Novikov, E. G. & VanAs, H. (2002) *J. Magn. Reson.* **156,** 213–221.
29. Kroenke, C. D., Ackerman, J. J. H. & Yablonskiy, D. A. (2004) *Magn. Reson. Med.* **52,** 1052–1059.
30. Chin, C. L., Wehrli, F. W., Fan, Y. L., Hwang, S. N., Schwartz, E. D., Nissanov, J. & Hackney, D. B. (2004) *Magn. Reson. Med.* **52,** 733–740.
31. Yablonskiy, D. A., Bretthorst, G. L. & Ackerman, J. J. H. (2003) *Magn. Reson. Med.* **50,** 664–669.
32. Sukstanskii, A. L., Yablonskiy, D. A. & Ackerman, J. J. H. (2004) *J. Magn. Reson.* **170,** 56–66.
33. Mulkern, R. V., Gudbjartsson, H., Westin, C. F., Zengingonul, H. P., Gartner, W., Guttmann, C. R. G., Robertson, R. L., Kyriakos, W., Schwartz, R., Holtzman, D. *et al.* (1999) *NMR Biol.* **12,** 51–62.
34. Maier, S. E., Bogner, P., Bajzik, G., Mamata, H., Mamata, Y., Repa, I., Jolesz, F. A. & Mulkern, R. V. (2001) *Radiology* **219,** 842–849.
35. Clark, C. A. & Le Bihan, D. (2000) *Magn. Reson. Med.* **44,** 852–859.
36. Buxton, R. B., Wong, E. C. & Frank, L. R. (1998) *Magn. Reson. Med.* **39,** 855–864.
37. Mangia, S., Giove, F., Bianciardi, M., Di Salle, F., Garreffa, G. & Maraviglia, B. (2003) *J. Neurosci. Res.* **71,** 463–467.
38. Lehericy, S., Biondi, A., Sourour, N., Vlaicu, M., du Montcel, S. T., Cohen, L., Vivas, E., Capelle, L., Faillot, T., Casasco, A., *et al.* (2002) *Radiology* **223,** 672–682.
39. Duong, T. Q., Yacoub, E., Adriany, G., Hu, X. P., Ugurbil, K. & Kim, S. G. (2003) *Magn. Reson. Med.* **49,** 1019–1027.
40. Le Bihan, D., Breton, E., Lallemand, D., Aubin, M. L., Vignaud, J. & Laval Jeantet, M. (1988) *Radiology* **168,** 497–505.
41. Inglefield, J. R. & Schwartz-Bloom, R. D. (1998) *J. Neurochem.* **71,** 1396–1404.
42. Takagi, S., Obata, K. & Tsubokawa, H. (2002) *Neurosci. Res.* **44,** 315–324.
43. Tasaki, I. (1999) *Jpn. J. Physiol.* **49,** 125–138.
44. Inoue, H., Mori, S. i., Morishima, S. & Okada, Y. (2005) *Eur. J. Neurosci.* **21,** 1648–1658.
45. Macvicar, B. A., Feighan, D., Brown, A. & Ransom, B. (2002) *Glia* **37,** 114–123.
46. Tasaki, I. & Byrne, P. M. (1990) *Biophys. J.* **57,** 633–635.
47. Metuzals, J. & Tasaki, I. (1978) *J. Cell. Biol.* **78,** 597–621.
48. Tasaki, I. & Byrne, P. M. (1992) *Biochem. Biophys. Res. Commun.* **188,** 559–564.
49. Tsukita, S., Tsukita, S., Kobayashi, T. & Matsumoto, G. (1986) *J. Cell. Biol.* **102,** 1710–1725.
50. Xu, X. H. N. & Yeung, E. S. (1998) *Science* **281,** 1650–1653.
51. Anderson, A. W., Xie, J., Pizzonia, J., Bronen, R. A., Spencer, D. D. & Gore, J. C. (2000) *Magn. Reson. Imaging* **18,** 689–695.
52. Jefferys, J. G. R. (1995) *Physiol. Rev.* **75,** 689–715.
53. Muller, V., Birbaumer, N., Preissl, H., Braun, C. & Lang, F. (2002) *Eur. J. Neurosci.* **15,** 528–538.